ENCIT 2018

ABCM Associação Brasileira de Engenharia e Ciências Mecânicas

17th Brazilian Congress of Thermal Sciences and Engineering
November 25th-28th, 2018, Águas de Lindóia, SP, Brazil

ENCIT-2018-0229
DOES THE INTRINSIC THREE-DIMENSIONALIZATION OF LAMINAR SEPARATION BUBBLES ENHANCE ITS AMPLIFIER CHARACTER?

Daniel Rodríguez
Laboratory of Theoretical and Applied Mechanics (LMTA), Graduate Program in Mechanical Engineering (PGMEC), Mechanical Engineering Department, Universidade Federal Fluminense, Niteroi, Brazil.
danielrodriguez@id.uff.br

Elmer M. Gennaro
São Paulo State University (UNESP), Campus São João da Boa Vista, São João da Boa Vista, SP, Brazil
elmer.gennaro@unesp.br

Leandro F. Souza
Institute of Mathematical and Computer Sciences, University of São Paulo, São Carlos-SP, Brazil.
lefraso@icmc.usp.br

Abstract. *Previous studies demonstrate laminar separation bubbles (LSB) in the absence of external disturbances or forcing are intrinsically unstable with respect to a three-dimensional instability of centrifugal nature. This instability produces topological modifications of the recirculation region with the introduction of streamwise vorticity in an otherwise purely two-dimensional time-averaged flows. Concurrently, the existence of spanwise inhomogeneities in LSBs have been reported in experiments in which the amplification of convective instability waves is seen to dominate the physics. The co-existence of the two instability mechanisms and its interactions are investigated here by means of three-dimensional Parabolized Stability Equations. The spanwise waviness of the LSB on account of the primary instability is found to modify the amplification of incoming disturbance waves in the linear regime, resulting in a staggered arrangement of the disturbances in the aft portion of the bubble, reminiscent of an oblique transition scenario.*
Keywords: *Laminar separation bubbles, Parabolized stability equations, Tollmien-Schlichting waves, Flow instability*

1. INTRODUCTION

Separation bubbles have the potential to amplify external disturbances in a explosive manner: the orders-of-magnitude amplitude growth resulting from convective instability mechanisms typically leads to strong non-linear phenomena and transition to turbulence, even at low excitation levels (Dovgal *et al.* (1994); Alam and Sandham (2000); Diwan and Ramesh (2009); Marxen *et al.* (2013)). Some researchers investigated the origin of three-dimensionality under these circumstances, attributing it mainly to secondary instabilities of the spanwise vortices shed from the bubble (Rist and Maucher (2002); Marxen *et al.* (2013)). Rist and Maucher (1994) investigated the non-linear interactions occurring when two oblique waves were excited, finding that the transition occurred in an abrupt manner (which they termed *oblique breakdown*) more similar to the experimental observations than under other forcing conditions in which the dominant component was 2D.

The absence of external excitation neglects the amplifier behavior of the bubbles, and only self-excited global instabilities have the potential of initiating the transition process. Recently (Rodríguez *et al.* (2013)) it was demonstrated that a 3D global instability mode becomes active for LSBs that are significantly weaker (with a reversed-flow magnitude $u_{rev} \sim 7-8\%$) than required for the onset of self-sustained two-dimensional oscillations ($u_{rev} \sim 16-20\%$) (Alam and Sandham (2000); Rist and Maucher (2002)). On the other hand, the presence of spanwise gradients in the 3D base flow as well as spanwise sections with a peak recirculation u_{rev} higher than that of the baseline 2D LSB suggests that the primary centrifugal instability can enhance the amplifier character of the separation bubbles. In this respect, it is worth noting that experimental and numerical studies observed the spontaneous appearance of streamwise streaks (Watmuff (1999); Spalart and Strelets (2000)) or three-dimensionality (Diwan and Ramesh (2009)) underlying the dominant convective instability and without explicitly imposing them.

This paper addresses the question of the possibly enhanced amplification of the externally imposed convective instabilities due to the three-dimensionalization of the initially 2D LSB. Section 2briefly reviews the properties of the primary instability and the resulting three-dimensional steady flow fields. An extension of the Parabolized Stability Equations (PSE) that considers three-dimensional (with one slowly-diverging direction) base flows, sometimes referred to as PSE-3D Herbert (1997); Broadhurst and Sherwin (2008), is described in section 3. Section 4shows some preliminary results

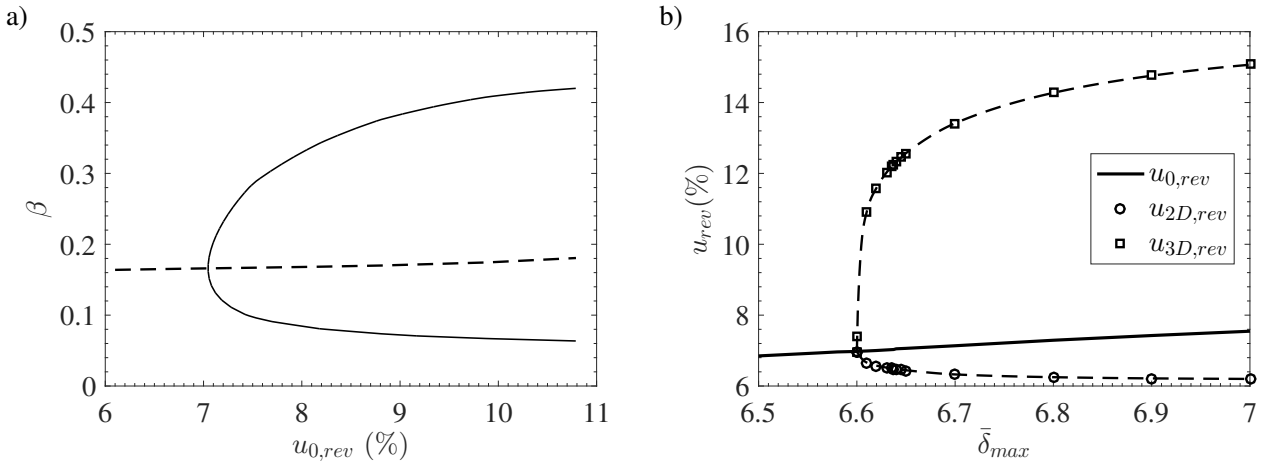

Figure 1. (a) Neutral curve for the primary instability eigenmode (solid line) and spanwise wavenumber of maximum growth rate (dashed line). (b) Bifurcation diagram of the primary instability, corresponding to the saturation of the three-dimensional instability. Peak reversed flow of the baseline LSB ($u_{0,rev}$, solid line without symbols), the saturated three-dimensional flow ($u_{3D,rev}$, squares), and the spanwise-averaged saturated flow ($u_{2D,rev}$, circles).

and conclusions.

2. SELF-EXCITED PRIMARY INSTABILITY

Following our previous works (Rodríguez and Theofilis (2010); Rodríguez *et al.* (2013); Rodríguez *et al.*), a family of LSBs on a flat-plate boundary layer is considered. Baseline LSBs are computed using an inverse nonsimilar boundary-layer formulation in which a streamwise distribution of the displacement thickness is prescribed. For a bounded streamwise extent, the displacement thickness is smoothly increased over the corresponding value for a zero-pressure-gradient boundary layer. The streamwise extent of the displacement thickness increase is fixed, and different decelerated flows are computed by varying the peak displacement thickness $\bar{\delta}_{max}$. Fully laminar, two-dimensional and steady flows with a closed recirculation region are computed in this manner.

The dimensionless form used in this work is defined with the free-stream velocity at the inlet section. The boundary-layer displacement thickness at a location upstream of the deceleration, where the flow corresponds to a zero-pressure-gradient, is used to scale distances. The Reynolds number based on this displacement thickness is 450, and the corresponding streamwise coordinate is $x = 152$.

Global eigenmode analyses, considering modal perturbations of the form $\hat{\mathbf{q}}(x, y) \exp[\mathrm{i}(\beta z - \omega t)]$, show that the three-dimensional centrifugal instability is the only self-excited linear mechanism active in the present baseline LSBs. Figure 1(a) shows the neutral curve and the dominant spanwise wavenumber β as a function of $u_{0,rev}$. This instability is characterized by: (i) its frequency $\omega = 0$; (ii) it is not active for two-dimensional perturbations; (iii) it has a preferential wavenumber $\beta_c \approx 0.166$ for the present LSBs; and (iv) it becomes active for reversed flow larger than $u_{0,rev} \approx 6.98\%$. Detailed information on the primary instability analyses can be found elsewhere (Rodríguez *et al.* (2013)).

Rodríguez *et al.* studied the nonlinear evolution subsequent to the onset of the three-dimensional instability using direct numerical simulations, and determined that it corresponds to a supercritical pitchfork bifurcation: the nonlinear interactions involving the fundamental wavenumber β_c, its harmonics and the distortion of the spanwise homogeneous low component result in the saturation of the disturbance growth and the formation of fully three-dimensional yet steady flows. The three-dimensional flows at saturated conditions are denoted by $\mathbf{q}_{3D}$ in what follows, while $\mathbf{q}_{2D}$ refers to their spanwise average. Figure 1(b) shows the bifurcation diagram: the peak reversed flow in the undisturbed baseline LSB $u_{0,rev}$, the three-dimensional saturated flow $u_{3D,rev}$ and its spanwise average $u_{2D,rev}$, as a function of the peak displacement thickness in boundary-layer units, $\bar{\delta}_{max}$. While the centrifugal instability reduces the mean bubble recirculation, the spanwise modulation of the separated shear layer results in localized peak reversed flow greater than $u_{3D,rev} = 10\%$.

3. MARCHING-PLANE PARABOLIZED STABILITY EQUATIONS (PSE-3D)

The classic Parabolized Stability Equations (PSE) (Herbert (1997)) recast the Navier-Stokes equations in disturbance form as a parabolic marching problem along the slow, streamwise coordinate X; the solution is computed at each cross-section by an iterative solution procedure that involves the solution of a number of one-dimensional linear problems, described by operators akin to the one-dimensional stability EVP. The classic PSE approach is extended here to three-dimensional base flows that depend strongly on two spatial directions and only mildly on the streamwise one: disturbances

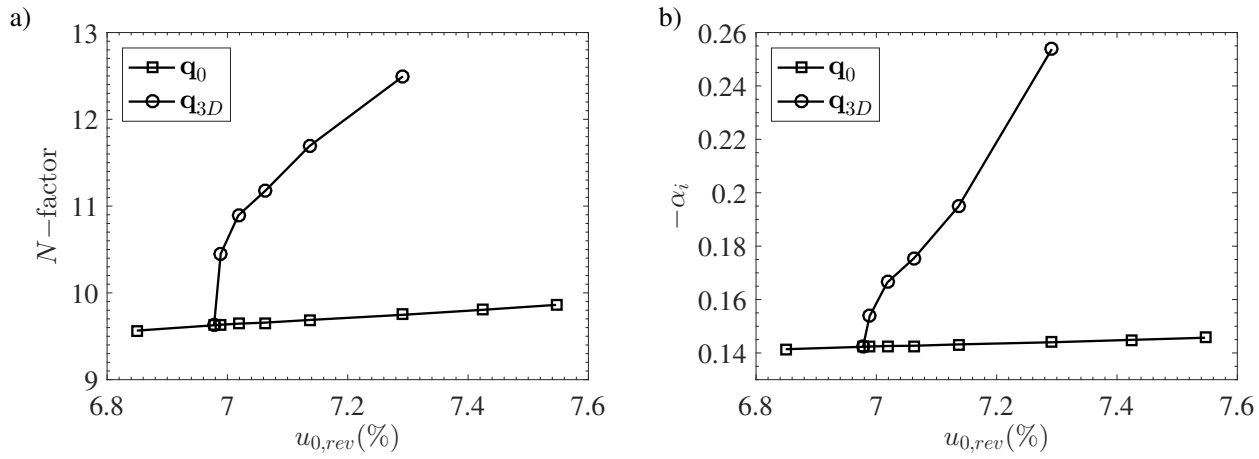

Figure 2. (a) Maximum $N-$factor and (b) maximum growth rate $-\alpha_i$ for baseline LSBs $\mathbf{q}_0$ and three-dimensional LSBs $\mathbf{q}_{3D}$, as a function of $u_{0,rev}$.

of the form

$$\mathbf{q}'(x,y,z,t) = \hat{\mathbf{q}}(X,y,z)\exp\left[\mathrm{i}(\int_{x'}\alpha(X')dx' - \omega t)\right] + c.c. \tag{1}$$

are considered, where $\hat{\mathbf{q}}(X,y,z)$ is the shape function and $\alpha(X')$ is a streamwise wavenumber which depends on the slow variable X. Introduction of this decomposition into the Navier Stokes equations in disturbance form, one obtains the matrix problem

$$\mathcal{R}\frac{\partial\hat{\mathbf{q}}}{\partial X} = \mathcal{L}\hat{\mathbf{q}} + \mathbf{F}(\hat{\mathbf{q}},\hat{\mathbf{q}}). \tag{2}$$

PSE can take into account non-linear interactions between the different frequency Fourier modes, through the coupling term $\mathbf{F}$. The marching algorithm in PSE requires of a normalization condition to isolate the slow variations of the shape function $\hat{\mathbf{q}}$ from the fast-scale oscillations and spatial growth. Here, the following normalization condition (Herbert (1997)) is used

$$\int_y\int_z \hat{\mathbf{q}}^*\frac{\partial\hat{\mathbf{q}}}{\partial X}\,dydz, \tag{3}$$

which provides an condition for the iterative calculation of α. The superscript $*$ denotes complex conjugation. This approach, being an straight-forward extension of the classic PSE, was not successfully implemented until Broadhurst and Sherwin (2008) due to its computational cost.

A new stability code is used Rodríguez and Gennaro (2017), that combines variable-stencil high-order finite differences and sparse algebra, exploiting the banded structure of the differentiation matrices. In this work, a 7-points stencil is used, which results in the optimal balance between convergence of results and computational cost. PSE are marched along the streamwise direction using an implicit Euler scheme. The necessary sparse matrix inversions are done using the package MUMPS Amestoy *et al.* (2001). Further details on the numerics can be found elsewhere Rodríguez *et al.* (2018); Rodríguez and Gennaro (under review).

4. RESULTS

The three-dimensional separation bubbles $\mathbf{q}_{3D}$ resulting from the saturation of the primary self-excited instability, and the baseline two-dimensional LSBs $\mathbf{q}_0$ are taken as the base flows $\bar{\mathbf{q}}$ in the analyses. The spatial local stability EVP described in section 3is applied to determine the initial conditions for the PSE integration. The arbitrary cross-section $x_0 = 100$ is chosen as inlet. The spanwise domain size is adjusted to be one wavelength of the primary instability, i.e. $L_z = \lambda_z = 2\pi/\beta_c$, and periodicity is imposed on this direction. The plane ($\beta = 0$) T-S wave for each ω is imposed as inlet conditions.

The convective amplification of the disturbance waves is quantified by the N-factor

$$N(x,\omega) = \log\left(\left|\frac{A(x)_\omega}{A(x_n)_\omega}\right|\right) = -\int_{x_n}^{x}\alpha_i(\xi,\omega)\mathrm{d}\xi, \tag{4}$$

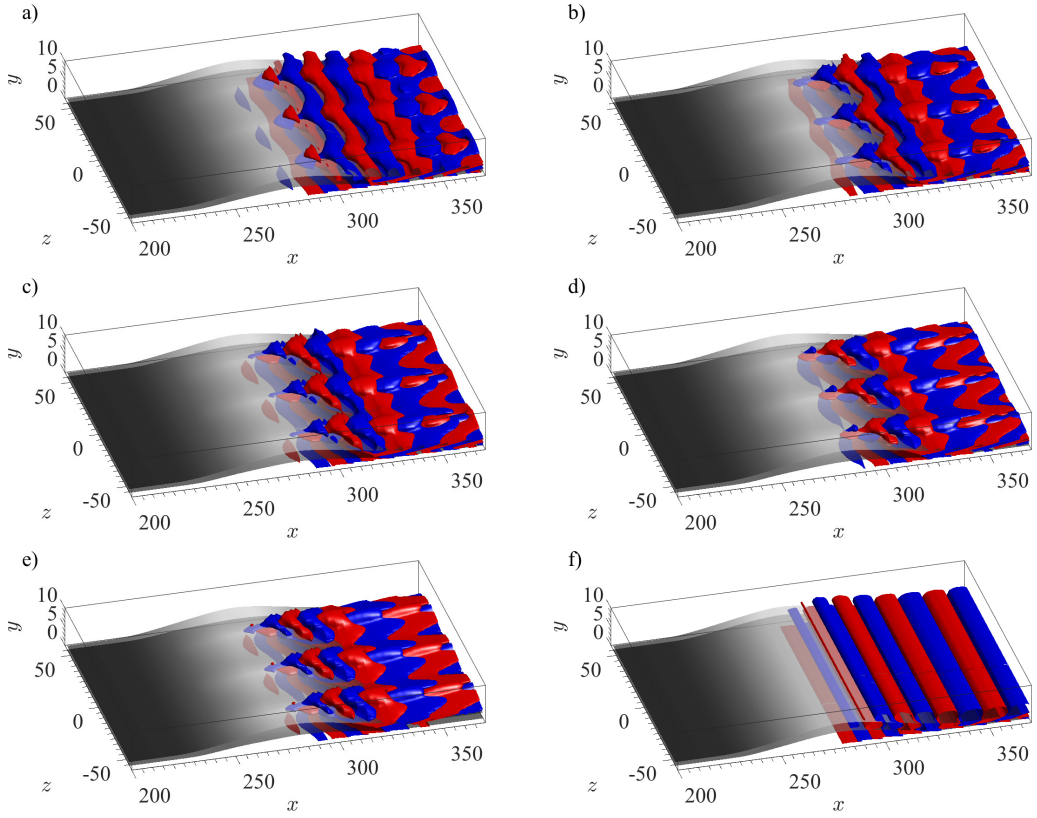

Figure 3. Baseline LSB and eigenmode corresponding to the primary instability. Grey surfaces correspond to $u_0 = 0$ and 0.5. The color surfaces correspond to $\omega_z' = \pm 0.1$ of the disturbance's spanwise vorticity component. The disturbance field is normalized with $\|\omega_z'\|_\infty = 1$. Three-dimensional LSBs for $u_{0,rev}$ (a) 6.99%, (b) 7.02%, (c) 7.06%, (d) 7.14%, (e) 7.29%; and (f) two-dimensional LSB for $u_{0,rev} 7.55\%$. The frequency for the maximum $N-$factor is considered for each case.

where x_n is the coordinate for the neutral conditions ($\alpha_i = 0$), different for each frequency ω.

The maximum $N-$factor computed for each separation bubble is shown in figure 2(a). The maximum amplification for the two-dimensional bubbles rises moderately from $N = 9.57$ ($u_{0.rev} = 6.85\%$) to $N = 9.86$ ($u_{0,rev} = 7.55\%$). Conversely, a remarkable increase in the maximum amplification follows from the three-dimensionality of the separation bubble, reaching values $N \approx 12.5$ for the base flow $\mathbf{q}_{3D}$ corresponding to $u_{0,rev} = 7.29\%$. Figure 2(b) shows the dependence of the maximum growth rate with the reversed flow for two- and three-dimensional base flows. Similarly to the $N-$factors, the moderate increase in the growth rate for the two-dimensional LSBs contrasts with the strong increase in the growth rate for three-dimensional bubbles.

The spatial structure of the disturbance waves corresponding to the maximum amplitude conditions is discussed next. Three-dimensional bubbles with $u_{0,rev} = 6.99-7.29\%$ and the two-dimensional LSB with higher reversed flow, $u_{0,rev} = 7.55\%$ ($\bar{\delta}_{max} = 7$), are shown in figure 3. The disturbance field is normalized with the maximum spanwise vorticity, and the surfaces correspond to $\omega_z' = \pm 0.1$. Disturbance waves, spanwise-homogeneous at introduction and upstream of separation, are distorted by the spanwise-varying separation bubble. Disturbance amplitude peaks are aligned with the spanwise planes of higher reversed flow, while the minimum disturbance amplitudes are aligned with the spanwise planes of lesser reversed flow. In the three-dimensional steady LSBs $\mathbf{q}_{3D}$, a positive streamwise streak follows downstream of the reversed-flow peak, which distorts the relative phases of the disturbance waves along the spanwise direction. The result resembles pairs of oblique waves, that seemingly arise from the peak reversed-flow locations in the figures.

Visual inspection of the 3D-PSE results indicate that the disturbances streamwise wavelength changes abruptly around the reattachment location for the three-dimensional LSBs. The maximum amplitudes are attained slightly downstream of reattachment, where the wavelengths are longer and typical of the attached boundary layer. Table 1 shows the real part of the wavenumber α_r inside the reversed flow region and after reattachment for the three-dimensional LSBs at their corresponding maximum amplitude frequency. The aspect ratio between the spanwise and streamwise periodicity lengths, $\lambda_z/\lambda_x = \alpha/\beta_c$, is also shown for each case. The streamwise wavelength in the reversed flow region downstream of the maximum wall-normal extent of the bubble, the streamwise wavenumber only a slight variation with $u_{0,rev}$, and the aspect ratio $\lambda_z/\lambda_x \approx 1.93 - 2.1$. These values are in excellent agreement with experimental visualizations using particle image velocimetry on LSBs formed on a flat plate (Michelis *et al.* (2018)) and on the lee-side of an airfoil (Kurelek *et al.* (2016)),

Table 1. Streamwise wavenumber and aspect ratio $\lambda_z/\lambda_x = \alpha/\beta_c$ of the oblique disturbance waves in the reversed flow region and just after reattachment, for the frequencies of maximum total amplitude. The frequency is also given in terms of the Strouhal number St_θ.

			After reattachment		Reversed flow	
$u_{0,rev}(\%)$	ω	St_θ	α_r	λ_z/λ_x	α_r	λ_z/λ_x
6.98	0.1284	0.0096	0.2995	1.804	0.3211	1.934
6.99	0.1264	0.0094	0.2540	1.530	0.3231	1.946
7.02	0.1300	0.0097	0.2310	1.392	0.3279	1.975
7.06	0.1313	0.0098	0.2264	1.364	0.3312	1.995
7.14	0.1339	0.0100	0.2221	1.338	0.3379	2.036
7.29	0.1390	0.0104	0.2143	1.291	0.3537	2.131

in which spanwise-modulated vortical structures were found to appear in the absence of explicit forcing.

Finally, table 1 also shows the frequencies corresponding to maximum amplitudes in terms of the Strouhal number defined using the momentum thickness and free-stream velocity at separation, in order to allow for comparison with other results in the literature. The Strouhal number for which the maximum amplitudes are attained lay in the range $St_\theta = 0.0094 - 0.0104$, which agrees well with the reported experimental measurements on unforced flat-plate LSBs (Serna and Lázaro (2014, 2015); Michelis *et al.* (2018)).

5. CONCLUSIONS

The primary instability sets in at reversed flows higher than $u_{0,rev} \approx 6.98\%$ and induces a spanwise-periodic modulation of the separation bubble in terms of size and recirculation intensity. The three-dimensionality of the separated shear layer impacts on the amplification of disturbance waves originated upstream. The total amplification is increased dramatically, with the maximum $N-$factor shifting from $N = 9.747$ to $N = 12.495$ for the same conditions.

The LSB's streamwise vorticity distorts the initially two-dimensional T-S waves periodically along the spanwise direction resulting into an arrangement that resembles pairs of oblique waves. The combination of the dominant streamwise wavenumber, determined by the convective instability of disturbance waves, and the spanwise wavenumber associated with the self-excited centrifugal instability, define an aspect ratio of the wavy disturbances in the aft portion of the separation bubble $\lambda_z/\lambda_x \approx 1.94 - 2.01$, which again agrees well with those observed in unforced experiments (Watmuff (1999); Kurelek *et al.* (2016); Michelis *et al.* (2018)). The organized oblique wave pattern together with the strong spatial amplification suggests an oblique transition scenario akin to that proposed by Rist and Maucher (1994).

6. ACKNOWLEDGMENTS

The authors acknowledge funding from CNPq (grants 405144/2016-4, 305512/2016-1, 423846/2016-7), FAPESP (grants 2014/24782-0, 2017/01586-0) and FAPERJ (grants 200003, 223669).

7. REFERENCES

Alam, M. and Sandham, N.D., 2000. "Direct numerical simulation of 'short' laminar separation bubbles with turbulent reattachment". *J. Fluid Mech.*, Vol. 410, pp. 1–28.

Amestoy, P.R., Duff, I.S., L'Excellent, J.Y. and Koster, J., 2001. "A fully asynchronous multifrontal solver using distributed dynamic scheduling". *SIAM J. Matrix Anal. Appl.*, Vol. 23, No. 1, pp. 15–41. ISSN 0895-4798.

Broadhurst, M. and Sherwin, S., 2008. "The parabolised stability equations for 3d-flows: implementation and numerical stability". *Applied Numerical Mathematics*, Vol. 58, No. 7, pp. 1017 – 1029.

Diwan, S. and Ramesh, O., 2009. "On the origin of the inflectional instability of a laminar separation bubble". *J. Fluid Mech.*, Vol. 629, pp. 263–298.

Dovgal, A., Kozlov, V. and Michalke, A., 1994. "Laminar boundary layer separation: instability and associated phenomena". *Prog. Aero. Sci.*, Vol. 3, pp. 61–94.

Herbert, T., 1997. "Parabolized stability equations". *Ann. Rev. of Fluid Mechanics*, Vol. 29, pp. 245–283.

Kurelek, J.W., Lambert, A.R. and Yarusevych, S., 2016. "Coherent structures in the transition process of a laminar separation bubble". *AIAA J.*, Vol. 54, No. 8, pp. 2295–2309.

Marxen, O., Lang, M. and Rist, U., 2013. "Vortex formation and vortex breakup in laminar separation bubbles". *J. Fluid Mech.*, Vol. 728, pp. 58–90.

Michelis, T., Yarusevych, S. and Kotsonis, M., 2018. "On the origin of spanwise vortex deformations in laminar separation bubbles". *J. Fluid Mech.*, Vol. 841, pp. 81–108.

Rist, U. and Maucher, U., 1994. "Direct numerical simulation of 2–d and 3–d instability waves in a laminar separation bubble". In B. Cantwell, ed., *AGARD-CP-551 Application of Direct and Large Eddy Simulation to Transition and Turbulence*. pp. 34–1 – 34–7.

Rist, U. and Maucher, U., 2002. "Investigations of time-growing instabilities in laminar separation bubbles". *Eur. J. Mech. B/Fluids*, Vol. 21, pp. 495–509.

Rodríguez, D. and Gennaro, E.M., 2017. "Three-dimensional flow stability analysis based on the matrix-forming approach made affordable". In J.S. Hesthaven, ed., *International Conference on Spectral and High-Order Methods 2016*. Springer, Lecture Notes in Computational Science and Engineering.

Rodríguez, D. and Gennaro, E.M., under review. "Enhancement of disturbance wave amplification due to the intrinsic three-dimensionalisation of laminar separation bubbles". *The Aeronautical Journal*.

Rodríguez, D., Gennaro, E.M. and Juniper, M.P., 2013. "The two classes of primary modal instability in laminar separation bubbles". *J. Fluid Mech.*, Vol. 734, p. R4.

Rodríguez, D., Gennaro, E.M. and Souza, L.F., ???? "Self-excited primary and secondary instability on laminar separation bubbles". *J. Fluid Mech., to be submitted*.

Rodríguez, D., Jotkar, M.R. and Gennaro, E.M., 2018. "Wavepacket models for subsonic twin jets using 3d parabolized stability equations". *Comptes Rendus Mec.*, Vol. in print.

Rodríguez, D. and Theofilis, V., 2010. "Structural changes of laminar separation bubbles induced by global linear instability". *J. Fluid Mech.*, Vol. 655, pp. 280–305.

Serna, J. and Lázaro, B.J., 2014. "The final stages of transition and the reattachment region in transitional separation bubbles". *Exp. Fluids*, Vol. 55, p. 1695.

Serna, J. and Lázaro, B.J., 2015. "On the bursting condition for transitional separation bubbles". *Aerosp. Sci. Technol.*, Vol. 44, pp. 43–50.

Spalart, P. and Strelets, M.K., 2000. "Mechanisms of transition and heat transfer in a separation bubble". *J. Fluid Mech.*, Vol. 403, pp. 329–349.

Watmuff, J.H., 1999. "Evolution of a wave packet into vortex loops in a laminar separation bubble". *J. Fluid Mech.*, Vol. 397, pp. 119–169.

8. RESPONSIBILITY NOTICE

The authors are the only responsible for the printed material included in this paper.